RSC Advances

This is an *Accepted Manuscript*, which has been through the Royal Society of Chemistry peer review process and has been accepted for publication.

Accepted Manuscripts are published online shortly after acceptance, before technical editing, formatting and proof reading. Using this free service, authors can make their results available to the community, in citable form, before we publish the edited article. This *Accepted Manuscript* will be replaced by the edited, formatted and paginated article as soon as this is available.

You can find more information about *Accepted Manuscripts* in the Information for Authors.

Please note that technical editing may introduce minor changes to the text and/or graphics, which may alter content. The journal's standard Terms & Conditions and the Ethical guidelines still apply. In no event shall the Royal Society of Chemistry be held responsible for any errors or omissions in this *Accepted Manuscript* or any consequences arising from the use of any information it contains.

ROYAL SOCIETY OF CHEMISTRY

www.rsc.org/advances

Cr-phthalocyanine monolayer as a potential catalyst for NO reduction investigated by DFT calculations

Jittima Meeprasert,[1] Anchalee Junkaew, [1] Nawee Kungwan,[2,*] Bavornpon Jansang,[3] Supawadee Namuangruk[1,*]

[1] *National Nanotechnology Center (NANOTEC), National Science and Technology Development Agency, Pathumthani, 12120, Thailand,*
[2] *Department of Chemistry, Faculty of Science, Chiang Mai University, Chiang Mai 50200, Thailand*
[3] *PTT Research and Technology Institute, PTT Public Company Limited, Phahonyothin Rd., Sanubtub, Wangnoi, Ayutthaya 13170, Thailand*

Abstract

The reaction mechanism of nitric oxide (NO) reduction to nitrous oxide (N_2O) and N_2 catalyzed by Cr-phthalocyanine sheet (CrPc) was investigated by periodic density functional theory (DFT). The results showed that direct NO dissociation on the catalyst is inhibited by large energy barrier owing to the difficulty on the direct cleavage of the strong NO bond. The dimer manner in which the two NO come to play is more preferred via the three competitive mechanistic pathways consisting of two Langmuir-Hinshelwood (LH1 and LH2) and one Eley-Rideal (ER). N_2O is produced from LH1 and ER with the activation barriers (Ea) of 0.35 and 1.17 eV, respectively, while N_2 is a product from LH2 with the Ea of 0.57 eV. All the three pathways are highly exothermic process. Based on the energetic aspect, LH1 is the kinetically and exothermically most favorable pathway (Ea of the rate-determining step is 0.35 eV). Therefore, we predict that NO can be easily reduced by CrPc at mild condition. In environmental implication, CrPc would be a promising catalyst for abatement of NO at low temperature.

Keywords: Cr-phthalocyanine, NO reduction, DFT, N_2O, Langmuir-Hinshelwood, Eley-Rideal

*Corresponding author. naweekung@gmail.com (N.K) and supawadee@nanotec.or.th (S.N.)

RSC Advances Accepted Manuscript

1. Introduction

The emission of hazardous gases from various sources such as the combustion of fuel, vehicles and industrial processes has caused increasing environmental problems.[1] Among them, nitrogen oxide (NO) as the most prominent pollutant, which is mainly emitted from the exhausts,[2] has long been known as one of the serious pollutants. It has manifold devastating effects on the atmosphere (ozone depletion) and ecosystems (source of acid rain) as well as on human health (harmful to the respiratory systems).[3] With these problems directly impacting on environment and human as well as to meet the criteria of all stringent emission regulations made by leading countries around the world, therefore, engineers, catalysis researchers, and environmental scientists have been challenging to develop more efficient engines and better deNOx technologies. Therefore, designing effectively catalytic materials in the deNOx systems that can remove or reduce NO molecules from the atmosphere have been intensively pursued. Noble transition metal catalysts such as Pt, Pd, Rh, and Au are commonly used for NO reduction.[4-11] However, these metals are generally expensive and toxic that might limit their large-scale application uses. Moreover, the O atom produced from the dissociation of NO strongly adsorbs on the catalysts which poisons the catalysts and thereby limiting the low-temperature activity especially for Pt-based catalysts.[12, 13] To overcome these problems, alternative catalytic materials have been exploring. Density functional theory (DFT) method has been used as a tool for searching of the potential candidates for NO decomposition. Recently, silicon-doped graphene[14], nitrogen-doped graphene[15], silicene[16], and metal phthalocyanines (MPcs)[17] have been suggested. By theoretical study, Zhang et al.[15] showed that the catalytic reduction of NO on the metal-free silicon-doped graphene is favorable through the NO dimer

RSC Advances Accepted Manuscript

mechanism. Xu et al.[16] reported that the removal of NO is feasible using silicene as an effective catalyst and two mechanisms for NO reaction were provided with a direct dissociation mechanism and a dimer mechanism. The $(NO)_2$ dimer formation on silicene was found to be both thermodynamics and kinetics and more favorable than the direct dissociation which is in agreement with the study by Zhang et al.[15], although the catalytic materials being considered are different.

MPcs have interesting properties because of their precisely-controlled distribution of central metal atoms. Uniform dispersion of metals on Pc can overcome the problem of metal clustering which is usually found in other substrates. The magnetic and catalytic properties of Pc have been intensively studied by DFT calculations.[7] Very recently, Wang et al. [18] used DFT calculations to search for low-cost catalyst for oxygen reduction reaction. They predicted that Fe-phthalocyanine (FePc) monolayer presents the good catalytic performance.[18] For the application to NOx gases, Nguyen et al[17] studied NO adsorption on MPc (M=Fe, Mn, Co) as potential sensor devices for detecting NO gas. They found that the electronic structures of metal atoms were very important in shaping the ground-state electronic near the Fermi level to accommodate the incoming NO gas. NO can strongly chemisorb to the metal atom with an N-bound configuration (M---NO) with the attribution of hybridization of the π^* orbitals of NO and the d-orbitals of those transition metals. Park et al.[19] also elucidated chemisorption nature of NO with copper phthalocyanine (CuPc) supported with graphene by scanning tunneling microscopy (STM) and DFT calculations. They suggested the functionalization of graphene with MPc would be a potential candidate for NO sensing platform. However, Nguyen et al.[17] and Park et al.[19] did not further investigate the possible NO reduction mechanism on those MPcs.

RSC Advances Accepted Manuscript

Using DFT calculations Li and Sun[20] predicted that CrPc monolayer was a potential candidate for low-temperature CO oxidation. This CrPc catalyst is superior to other noble metals or metal loaded on carbon substrates in both catalytic activity and withstanding to CO and O poisoning. The calculated activation barrier of the rate-limiting step of the CO oxidation is very low at 0.55 eV (see **Table 1**), which is comparable to those of TiO_2(110) or MgO(110) supported Au nanoparticles model (0.35~0.75 eV)[21, 22] or free-standing Au nanoparticles (0.46~1.03 eV)[7, 23] using the same level of theory. The recent successes in theoretical prediction on mechanisms of the CO oxidation catalyzed by the CrPc sheet by Li and Sun[20] as well as the potential candidate of MPc for NO chemical sensors[17] mentioned above have inspired us to employ the CrPc as the candidate catalyst for NO reduction. To the best of our knowledge, its corresponding reaction mechanisms have not been investigated yet. With this inspiration then important questions arise naturally: can CrPc be used as a catalyst for NO reduction? If it can, is the mechanism similar to the reduction of NO on silicon-doped graphene[14] or NO on silicene[16] or the oxidation of CO on CrPc?[20] Can the NO reduction by CrPc be proceeded under low temperature range? Therefore in this work, we will provide the systematic answers to these questions by using the periodic DFT calculations.

2. Method of calculation

The spin-polarized DFT calculations were performed using the Dmol^3 module[24, 25] of Material Studio 8.0. The geometry optimizations, charge analysis, transition state locating and vibrational mode analysis were performed using the generalized gradient approximation (GGA) of Perdew−Burke−Ernzerholf (PBE) functional[26] for the exchange-correlation terms. The double numerical plus polarization (DNP) basis set[25] was employed with the real space global orbital

RSC Advances Accepted Manuscript

cutoff radius as 4.8 Å and the smearing of electronic occupations was set to be 5.0 x 10^{-3} Ha for ensuring the high quality results. All-electron calculations were performed for the C, N, O, and H atoms, and relativistic effect included effective potential was used to represent core electrons of the Cr atom. During the geometry optimizations, no symmetry constraints were imposed and the threshold was set to be 1.0 x 10^{-5} Ha in energy, 2.0 x 10^{-3} Ha $Å^{-1}$ in force, 5.0 x 10^{-3} Å. All self-consistent field (SCF) calculations were carried out with the convergence criterion of 1.0 x 10^{-5} Ha.

We set the *z*-direction perpendicular and the *x* and *y* directions parallel to the plane of the CrPc monolayer, and adopted a supercell length of 15 Å in the *z* direction to avoid the artificial interaction of periodic images, see **Figure 1**. The Brillouin zone was sampled with a 5 x 5 x 1 k-points. The transition state (TS) was searched by using the linear synchronous transit (LST) method, followed by repeated conjugated gradient (CG) refinements, and then quadratic synchronous transit (QST) maximizations[27] and repeated CG refinements until the TS is located. The nudged elastic band (NEB) method[28] was further employed to obtain the minimum energy pathway (MEP). The vibrational frequency calculation was performed on the obtained TS structure to ensure that it has only one imaginary frequency corresponding to the reaction coordinate.

In order to find the stable sites of NO on CrPc, the adsorption energy of different orientation of NO and adsorption sites (a metal, N or C) were performed. The calculated results show that the NO molecule strongly adsorbs on the metal site but weakly adsorbs on other non-metal sites. For NO adsorption on metal site of CrPc, the adsorption energies of the most stable positions of N-bound and O-bound orientations were calculated based on the following expression: $\Delta E = E_{\mathrm{CrPc+NO}} - (E_{\mathrm{CrPc}} + E_{\mathrm{NO}})$, where $E_{\mathrm{CrPc+NO}}$, E_{CrPc}, and E_{NO} are the total energies of the

RSC Advances Accepted Manuscript

CrPc−NO complex system, the free CrPc monolayer and the free NO molecule in the gas phase, respectively.

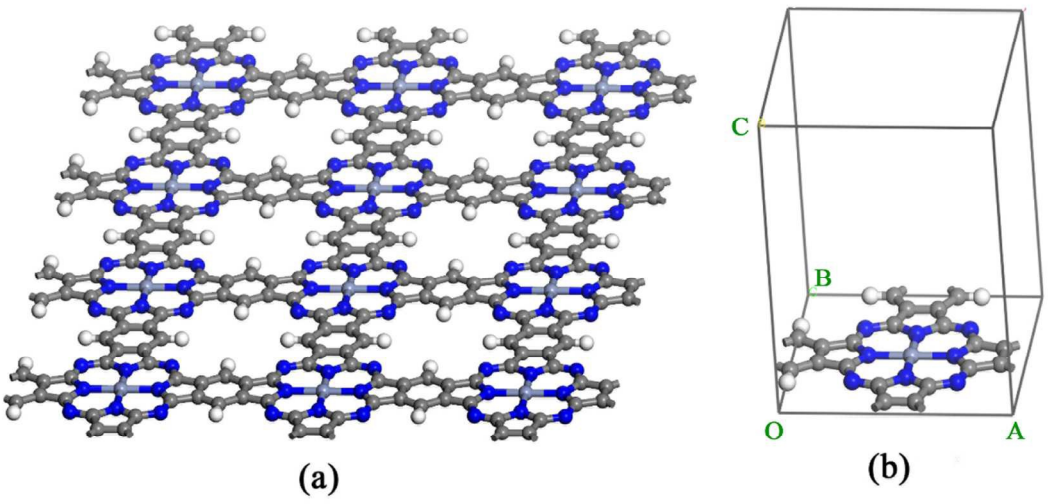

Figure 1. (a) CrPc monolayer and (b) unit cell of CrPc. The dark gray, blue, white and light blue balls represent C, N, H, and Cr atoms, respectively.

3. Results and Discussion

3.1 Adsorption of NO molecules on CrPc monolayer

NO adsorption on CrPc is determined in this part. Structural parameters and electronic charge properties were analyzed. In the bare CrPc sheet, the distances between the Cr atom and the four neighboring N atoms (Cr−N) are equivalent at 1.98 Å, which is in good agreement with previous studies.[20] The nature of electronic structure was analyzed in terms of the highest occupied molecular orbitals (HOMO) and the lowest unoccupied molecular orbitals (LUMO) of both CrPc and NO. The results are illustrated in Figure 2. The LUMO displays the strong d-orbital characteristics of the Cr atom, allowing an incoming electron to occupy this state. Therefore, with incoming electron from NO molecule, the strong forming bonds between N and O atoms of NO to the Cr atom of CrPc are considered.

RSC Advances Accepted Manuscript

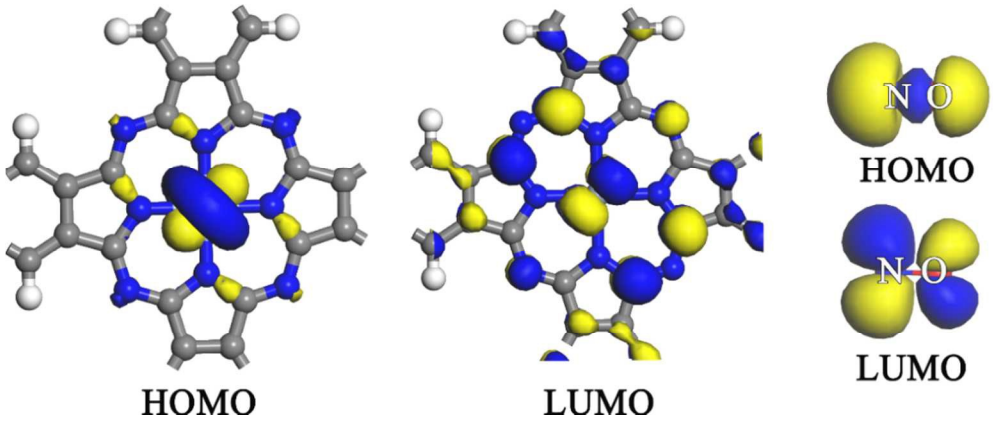

Figure 2 HOMOs and LUMOs of CrPc catalyst and nitric oxide.

The most stable structures of N-bound and O-bound modes of adsorbed NO on CrPc are depicted in Figure 3. In Figures 3a-b, the most stable orientation of both modes is linear and the N−O bond is elongated from 1.16 Å (in free NO) to 1.18 and 1.19 Å for N-bound and O-bound modes, respectively. The N−Cr bond (1.67 Å) is found to be shorter than O−Cr bond (1.78 Å) due to the larger binding energy of N-bound (-2.07 eV) compared to that of O-bound (-0.37 eV).The bonding interaction between NO molecule and CrPc can be described by the interaction between the LUMO of CrPc on the dπ and the 2π* orbitals of NO is favored as illustrated in Figure 2, which is similar to the interaction of NO on MnPc.[17] The N or O terminal of NO molecule can bind with Cr on the CrPc monolayer through the favorable symmetrical orbital. Figures 3c-d show the electron density difference plot of N- and O-bound adsorption modes. The yellow and purple colors represent electron depletion and accumulation after adsorption, respectively. At the N-bound mode (Figure 3c), it clearly demonstrates that after NO adsorbed on CrPc, electron density of the N=O bond is decreased while that of the intermolecular interaction area (N---Cr) is increased as seen by the yellow and purple regions, respectively. These

RSC Advances Accepted Manuscript

correspond to the elongating and shortening of the bonds described above. The same behavior is found for the O-bound mode. The larger purple region at the intermolecular area of the N-bound mode compared with the O-bond mode supports the shorter N−Cr bond than the O-Cr bond, and results in the stronger binding energy of the N-bound mode. Furthermore, the binding strength of N-bound mode of NO on CrPc is comparable to the N-bound mode of NO with other MPc such as MnPc-NO (E_{ad}=-1.73 eV), FePc-NO (E_{ad}=-1.90 eV), and CoPc-NO (E_{ad}=-1.55 eV), calculated by DFT method.[17] The O-bound mode has not been reported before on MPcs because its binding strength is quite weak. However, our study indicates that this O-bound mode becomes very important toward NO reduction when two NO molecules come to play together on the CrPc catalyst via a dimer mechanism as discussed in next section.

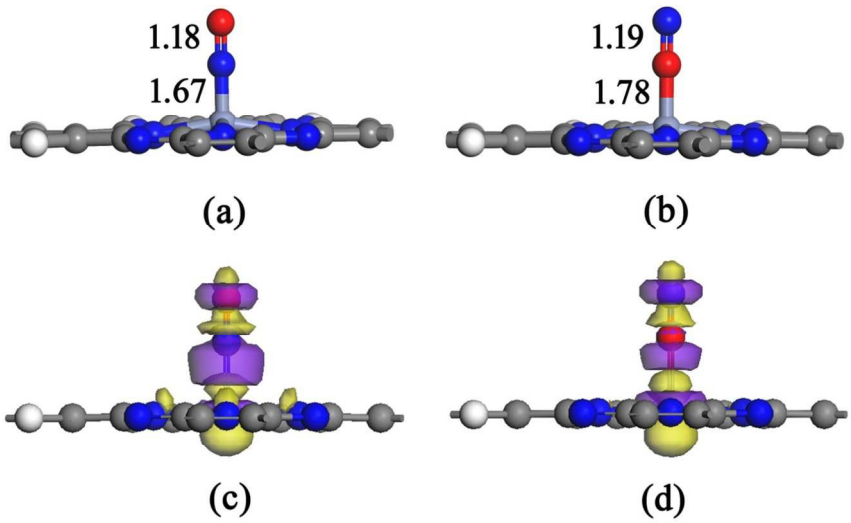

Figure 3 Structures of (a) N-bound and (b) O-bound modes of nitric oxide adsorbed on CrPc catalyst, and their corresponding electron density difference (c) and (d). Yellow and purple regions represent electron density depletion and accumulation, respectively.

RSC Advances Accepted Manuscript

To understand insight into the electronic properties of CrPc while it adsorbs NO molecule, the partial density of states (PDOS) for the N-bound mode of NO adsorbed on the CrPc are calculated. Figure 4 clearly shows that there is a strong hybridization between the Cr-d orbitals and NO orbitals in both spin-up and spin-down states which supports the electron density results above. Especially, in the spin-down states the 2π* orbital of NO molecule is dominantly occupied. This confirms that CrPc can activate NO molecule and sufficiently facilitate the further reaction.

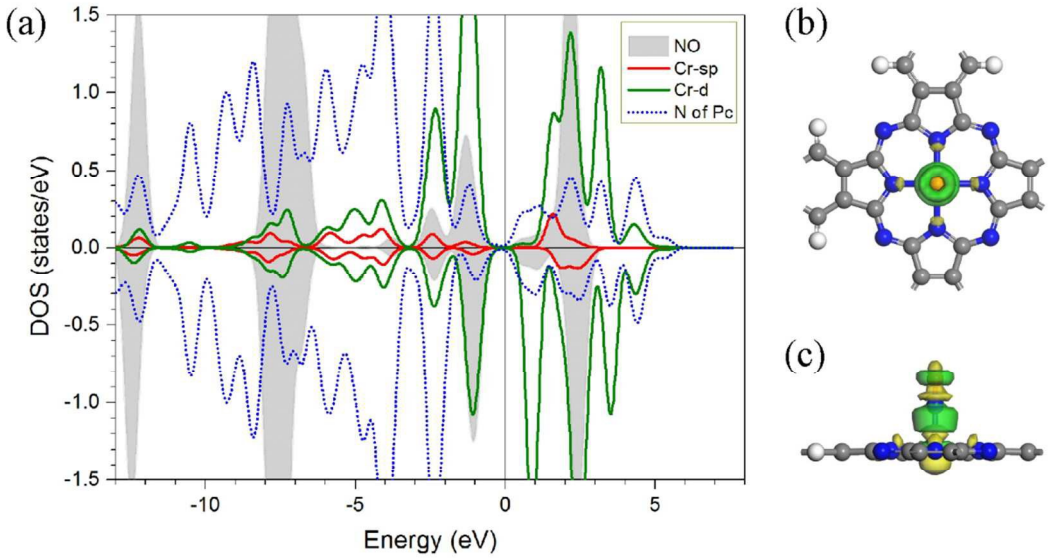

Figure 4 (a) Partial density of states (PDOS) of the NO adsorbed on CrPc monolayer and corresponding optimized structure on (b) top view and (c) side view

The possible ways of NO adsorption onto CrPc are presented in Figure 5. This step is considered as the important step because it controls the further step of the reaction pathway namely Langmuir-Hinshelwood (LH) and Eley-Rideal (ER) mechanisms. The formation of NO dimer on the metal-based catalytic materials during the NO reduction has been reported in

RSC Advances Accepted Manuscript

previous studies,[14-16, 29-34] in which the formation of gas-phase NO dimer from monomeric NO was first characterized by Dinerman and Ewing in 1970.[35] As depicted in Figure 5, two different dimer-intermediates are formed from the three different adsorption aspects denoted as initial states (**IS**), **IS1** for O-bound and O-bound interaction (Figure 5a, later leading to LH1 and LH2 pathways), **IS2** for N-bound and N-bound interaction (Figure 5b, later leading to ER pathway), and **IS3** for N-bound and O-bound interaction (Figure 5c). It is noted that only **IS1** and **IS2** can lead to the stable dimer intermediates, **Int1** and **Int2**, respectively. Under thermal equilibrium **IS3** can easily be converted to **IS2**, leading to the formation of **Int2**. The similarity and the differences between **Int1** and **Int2** structures are compared. As a result, NO molecules in these two intermediates similarly interact through a N−N bond. Differently, the five-membered ring of both N−O to CrPc is formed in the case of **Int1** while opened one side of the N−O is observed in the case of **Int2**. The further detailed information on NO reduction via the three pathways (LH1, LH2 and ER) will be discussed in the next section.

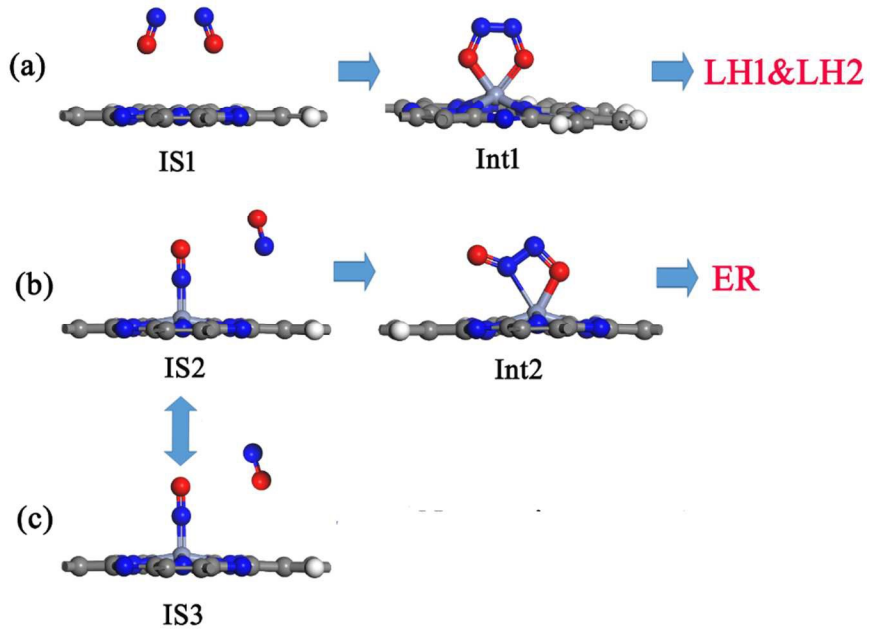

RSC Advances Accepted Manuscript

Figure 5. Coadsorption of two NO molecules on CrPc catalyst (a) O-bound and O-bound, (b) N-bound and N-bound, and (c) N-bound and O-bound.

3.2 Reduction of NO molecules on CrPc monolayer

The NO reduction mechanisms in many catalysts were proposed in previous reports[14, 30, 32, 36-38] which the reduction can occur through two possible reaction manners: (1) the direct NO dissociation, giving N and O adatoms; and (2) the dimer manner for NO reduction on a catalyst in which two adsorbed NO molecules interact with each other, yielding N_2O or N_2. In this study, the dimer manner proceeding via both Langmuir-Hinshelwood (LH) and Eley-Rideal (ER) mechanisms were systematically investigated for finding the favorable pathway. The direct NO dissociation was also examined to be compared with the dimer manner.

3.2.1 Direct NO dissociation

The direct NO dissociation was carefully checked and the result indicate that it is most likely not to take place on CrPc, which is similar to the NO reduction catalyzed by Si-doped graphene reported by Chen et al.[14] This unfavorable pathway is required high energy barrier (2.52 eV) and endothermicity as given in Figure 6. It is seen that to overcome the direct dissociation of a very strong NO bond, the NO adsorbs on the Cr with bidentate mode (**IS**). The transition state (**TS**) clearly shows the being broken of N=O bond which is elongated from 1.26 to 2.02 Å. Then, the dissociation is achieved after the O moves to form a three-membered ring with Pc counterpart (**FS**), which is very unstable. This pathway is thus very unlikely to happen.

RSC Advances Accepted Manuscript

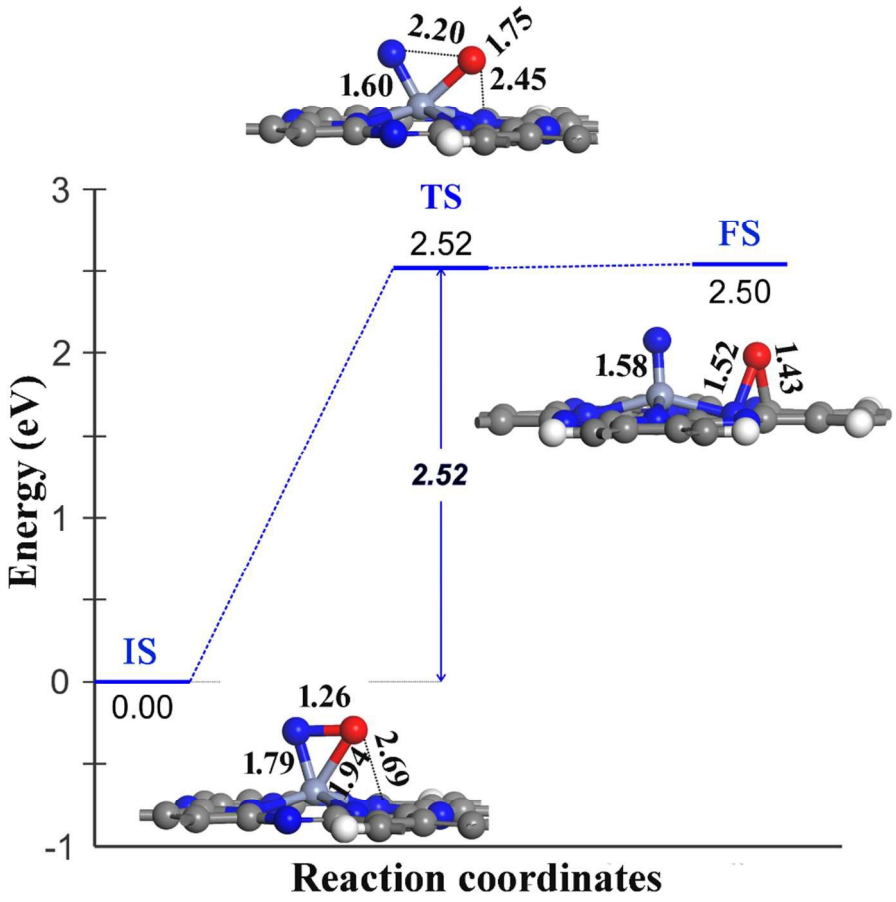

Figure 6. Energy diagram of direct NO dissociation on CrPc monolayer.

3.2.2 Langmuir Hinshelwood (LH) mechanism

The reaction pathways in the dimer manner are presented in this part. Figure 7 compares the potential energy surface (PES) diagram of LH mechanism which consists of two mechanistic pathways; LH1 and LH2. LH1 presents the reaction coordinates of the NO reduction to yield N_2O molecule (purple line) while LH2 generates N_2 and O_2 as the products (red line). The geometries of initial, intermediate and final states with labeled distance parameters are presented in Figure 7. Starting from structure **IS1** to form **Int1** through the transition state 1 (**TS1**), the intermolecular distances of N−N and the N−O of co-adsorbed NO molecules bound to the CrPc

RSC Advances Accepted Manuscript

are 1.96 and 1.17 Å, respectively, which are slightly shorter and longer than those of N_2 and NO molecules in the gas phase (1.97 and 1.16 Å), respectively. At the **TS1** state, decreasing of the distance between two NO and CrPc with the intermolecular distances of 2.67 and 2.62 Å can be observed. The NO bond lengths are lengthened to 1.19 Å while the N---N distance is shortened from 1.96 to 1.78 Å, indicating the forming of the five-membered ring intermediate. This step requires a very small energy of 0.02 eV. After **Int1** is formed by the cyclic formation of NO dimer in a cis-form, two possible paths are proposed to form N_2O (LH1) and N_2 (LH2). As a result, the LH1 is more favorable than another path due to higher exothermic and kinetic process. The LH1, which starts from **Int1** and leads to N_2O product, requires energy of 0.35 eV for forming **TS3** intermediate with one N−O bond being elongated from 1.35 to 1.75 Å before converging to **FS2**. The frequency calculation of **TS3** shows that it has a single imaginary frequency (-368.0 cm^{-1}), corresponding to the dissociation of one N−O bond of the adsorbed NO dimer (see detail of **TS3** in Figure 7). In the **FS2** state, N_2O is weakly bound and released, while one O atom is chemisorbed on CrPc with bond length of 1.56 Å. This O atom can be easily reduced by incoming CO molecule with 0.46 eV of activation barrier.[20]

For LH2 pathway, **Int1** can be converted into **FS1** giving out the N_2 molecule through the transition state **TS2**. An energy barrier of this path is 0.57 eV, which is 0.22 eV higher than that of LH1. For **TS2**, both O−Cr bonds (1.74 Å) which are shorter than those of **Int1** and the N−O bonds (1.65 and 1.67 Å) are almost separated from the O−Cr bonds. After releasing the N_2 molecule, **FS1** can thermally be converted to **RS1**, in which **RS1** can further yield O_2 molecule by breaking the O−Cr bonds. This step requires energy of 1.13 eV for O_2 desorption. In comparison, the LH2 pathway is obviously less favorable than the LH1 pathway in both terms of kinetic and thermodynamic.

RSC Advances Accepted Manuscript

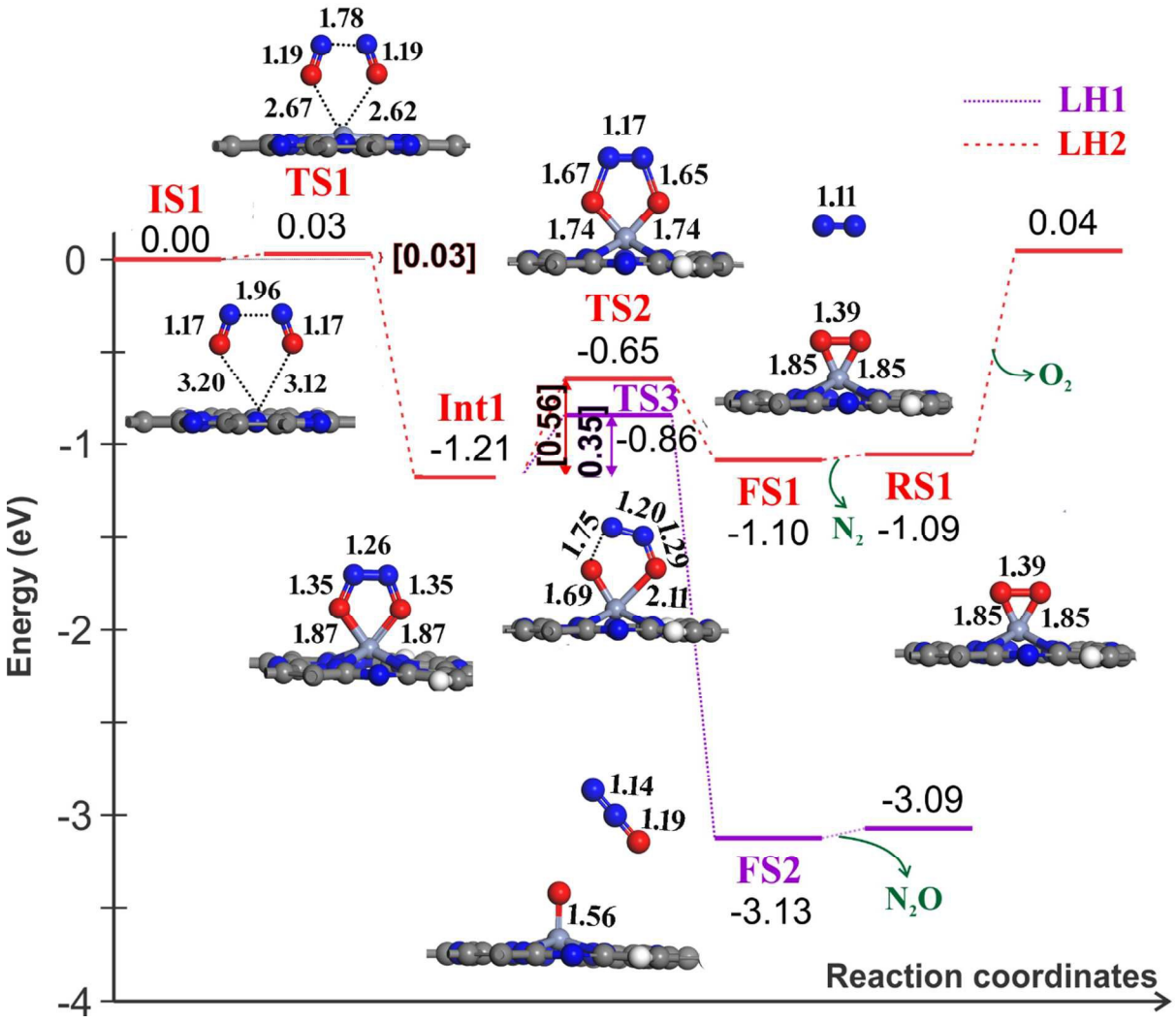

Figure 7 The LH potential energy diagram of NO reduction to N_2O formation (LH1, purple line) and N_2 formation (LH2, red line).

3.3.3 Eley-Rideal (ER) mechanism

The reduction of NO molecules through the ER mechanism is examined in this part. Depicted in Figure 8 is the obtained PES along the reaction coordinate of N_2O formation, as well as the corresponding initial, transition and final sates. At the **IS2** state, another NO molecule approaches the pre-adsorbed NO on CrPc with 1.67 Å of N−Cr bond. The NO dimer

RSC Advances Accepted Manuscript

intermediate (**Int2**) can be achieved through the formation of the **TS4** intermediate, requiring energy about 1.17 eV to connect the incoming NO molecule to the pre-adsorbed NO on CrPc. By considering the bonding between Cr and interacting atoms, the N−Cr bond is elongated from 1.94 Å to 2.16 Å, while the O−Cr bond is decreased from 2.50 Å to 1.85 Å as conversion of **TS4** to **Int2** step. The imaginary frequency of this transition state confirms a mode corresponding to the incoming O atom on the NO dimer to bond with Cr of CrPc. The N−O bond (1.37 Å) of the **Int2** is now longer than that in the **IS2** (1.16 Å) and **TS4** (1.24 Å). The **Int2** formation process is highly endothermic (1.44 eV) because of its constraint of four-membered ring structure. The unstable **Int2** can be easily transformed via **TS5** to **FS3** with a small energy barrier of 0.30 eV, yielding the N_2O molecule. The transformation of **Int2** requires the rupture of the already elongated N−Cr bond (2.16 Å) to free the one end of the NO dimer bound to CrPc (see detail of **TS5** in Figure 8). The process of forming stable **FS3** is very exothermic (3.33 eV). Finally, within the thermal equilibrium, the **FS3** having N_2O weakly bound on O-CrPc can release the N_2O molecule and the NO reduction to N_2O in ER mechanism is complete.

In the catalytic processes, a comparison of the overall barrier is commonly more important than a single-step barrier in each pathway. From the comparisons of the three energetic pathways on dimer manner, Figure 9, we found that all three pathways (LH1, LH2 and ER) are exothermic and possible. The comparison of the barriers of those three pathways leads to the conclusion that the reaction is the most likely to proceed through LH1 and therefore N_2O gas is predicted as the major product of the NO reduction on CrPc catalyst. With the very small barriers requiring of the LH1 (0.03 and 0.35 eV for the first and second steps, respectively), we predict that CrPc catalyst can catalyze this reaction in a low temperature range.

RSC Advances Accepted Manuscript

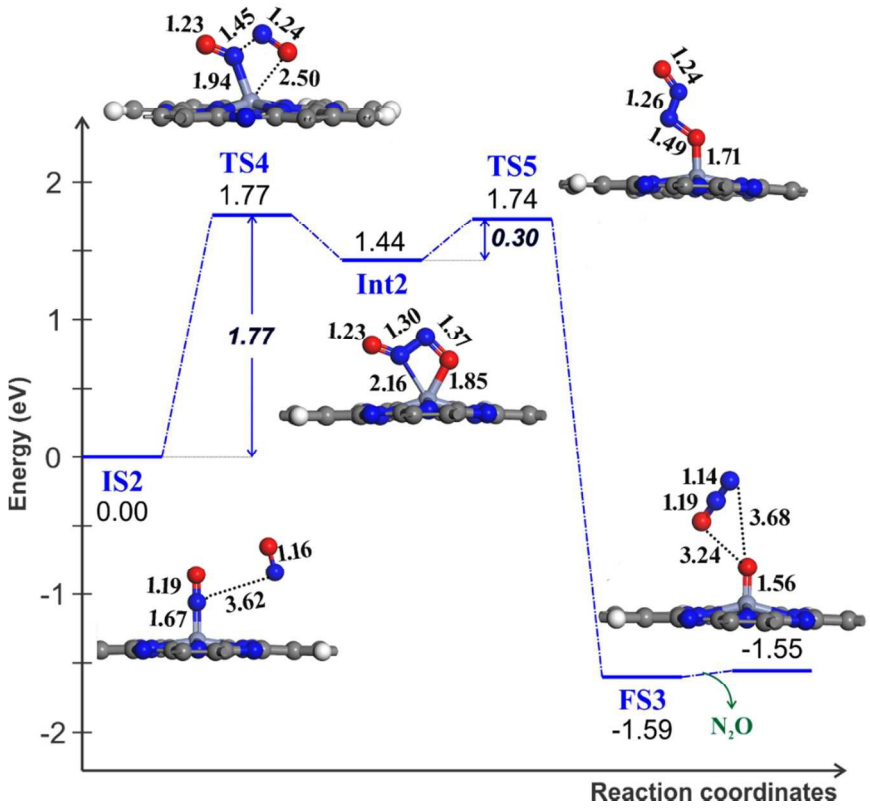

Figure 8 The potential energy surface diagram of N_2O formation via ER mechanism.

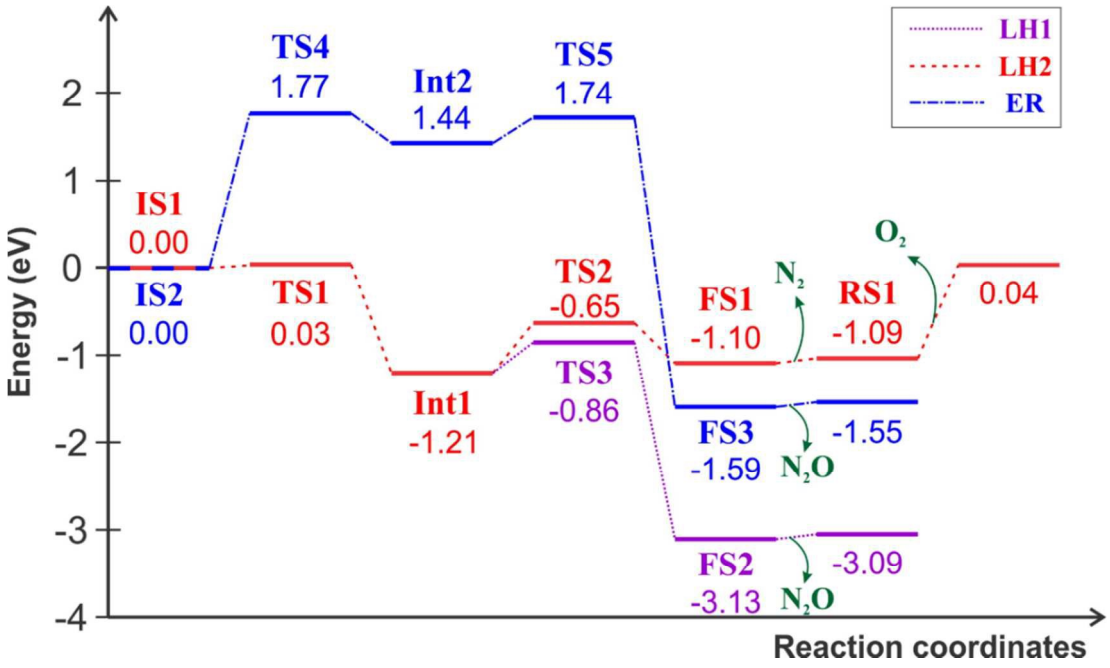

Figure 9 The PES diagram showing LH1, LH2, and ER pathways.

RSC Advances Accepted Manuscript

3.3.4 Calculated energy barrier comparison between CrPc and other catalytic materials

The calculated energy barriers at rate-limiting steps of NO and CO oxidation/reduction on various catalyst are summarized in Table 1 for convenient comparison. Those calculated values are in range of 0.35-0.76 eV depending on catalytic materials except for CO oxidation on Pt deposited on N doped graphene; the reaction proceeds with a very small energy barrier of 0.15 eV. It is clearly seen that our calculated barrier for the rate-limiting step at 0.35 eV along the most favorable LH1 pathway is found to be smaller than the NO reduction to N_2O catalyzed by silicon-doped graphene at 0.46 eV using the same level of theory.[14] Furthermore, by comparison the catalytic activity of CrPc to CO oxidation and NO reduction, it is found that in this study CrPc can catalyze NO reduction faster than CO oxidation with an energy barrier of 0.55 eV investigated by Li et al.[20] Therefore, CrPc is predicted as a potential catalytic material for low-temperature NO reduction. This is important because reduction of NO in low temperature is a crucial process in the context of air purification.

Table 1. The calculated energy barrier at rate-limiting step for the NO and CO decomposition reactions on various proposed catalysts.

Model	**Reaction steps**	**Barrier (eV)**
CrPc (This work)	$NO+NO \rightarrow NO_2 + O^*$	0.35
CrPc[20]	$2CO+O_2 \rightarrow 2CO_2$	0.55
Si-Graphene[14]	$NO+NO \rightarrow N_2O+O^*$	0.46
Pt/Ti-Porphyrin[39]	$CO+O_2 \rightarrow CO_2+O^*$	0.55
SiC[40]	$NO+NO \rightarrow N_2O$	0.72
Silicene[16]	$N_2O \rightarrow N_2+O^*$	0.45
Pt-Graphene[41]	$CO + O^* \rightarrow CO_2$	0.46
Pt-O/Graphene[42]	$CO+O_2 \rightarrow CO_2+O^*$	0.76

RSC Advances Accepted Manuscript

Pt-N doped Graphene[1]	$CO + O^* \rightarrow CO_2$	0.15

4. Conclusion

By employing the periodic DFT calculations with PBE functional, the reduction of NO molecules on CrPc monolayer has been investigated. The direct dissociation mechanism of NO, generally proposed on noble metal surfaces and metal-doped carbon materials, was found to be unfavorable because of the extremely high barrier and endothermic process. Whereas, the catalytic process of NO reduction via the NO dimer yielding N_2O molecules in both LH and ER mechanisms are more likely to occur because of lower energy barrier and their exothermic processes. Moreover, the N_2O formation through LH is more favorable than ER. Based on the same level of theory, the catalytic activity of CrPc toward NO reduction is higher than that of silicon-doped graphene[13] and our predicted NO reduction on CrPc is found to be more efficient than CO oxidation under the same condition.[19] Therefore, the insight understanding obtained from this work might be helpful to provide a guidance to develop catalytic materials for NOx abatement. MPcs-based catalysts, which is controllable dispersed of central metal, may open a new way in development of promising catalysts to overcome the problems encountered from existing commercial catalysts for air purification.

Acknowledgements

The authors wish to thank the National Nanotechnology Center (NANOTEC) through "the Flagship Clean Air Program" and Thailand Research Fund for financial support. Chiang Mai University, Chiang Mai is also acknowledged.

Notes and References

RSC Advances Accepted Manuscript

1. Y. Li, S. H. Chan and Q. Sun, *Nanoscale*, 2015, **7**, 8663-8683.
2. S. Roy and A. Baiker, *Chemical Reviews*, 2009, **109**, 4054-4091.
3. A. Fritz and V. Pitchon, *Applied Catalysis B: Environmental*, 1997, **13**, 1-25.
4. A. Alavi, P. Hu, T. Deutsch, P. L. Silvestrelli and J. Hutter, *Phys. Rev. Lett.*, 1998, **80**, 3650-3653.
5. Z.-P. Liu and P. Hu, *J. Chem. Phys.*, 2001, **115**, 4977-4980.
6. Z.-P. Liu, P. Hu and A. Alavi, *J. Am. Chem. Soc.*, 2002, **124**, 14770-14779.
7. G. Zhu and Q. Sun, *Computational Materials Science*, 2016, **112**, 492-502.
8. R. Toyoshima, M. Yoshida, Y. Monya, Y. Kousa, K. Suzuki, H. Abe, B. S. Mun, K. Mase, K. Amemiya and H. Kondoh, *J. Phys. Chem. C*, 2012, **116**, 18691-18697.
9. W. Yu, M. D. Porosoff and J. G. Chen, *Chem. Rev.*, 2012, **112**, 5780-5817.
10. R. Siburian, T. Kondo and J. Nakamura, *J. Phys. Chem. C*, 2013, **117**, 3635-3645.
11. S. Shan, V. Petkov, L. Yang, J. Luo, P. Joseph, D. Mayzel, B. Prasai, L. Wang, M. Engelhard and C.-J. Zhong, *J. Am. Chem. Soc.*, 2014, **136**, 7140-7151.
12. K. C. Taylor, *Catal. Rev.*, 1993, **35**, 457-481.
13. M. Shelef and G. W. Graham, *Catal. Rev.*, 1994, **36**, 433-457.
14. Y. Chen, Y.-j. Liu, H.-x. Wang, J.-x. Zhao, Q.-h. Cai, X.-z. Wang and Y.-h. Ding, *ACS Applied Materials & Interfaces*, 2013, **5**, 5994-6000.
15. X. Zhang, Z. Lu, Y. Tang, Z. Fu, D. Ma and Z. Yang, *Physical Chemistry Chemical Physics*, 2014, **16**, 20561-20569.
16. X. Xu, J. Li, X. Zhang, H. Xu, Z.-F. Ke and C. Zhao, *RSC Advances*, 2015, **5**, 22135-22147.
17. T. Q. Nguyen, M. C. S. Escaño and H. Kasai, *The Journal of Physical Chemistry B*, 2010, **114**, 10017-10021.
18. Y. Wang, H. Yuan, Y. Li and Z. Chen, *Nanoscale*, 2015, **7**, 11633-11641.
19. J. H. Park, J. E. Royer, E. Chagarov, T. Kaufman-Osborn, M. Edmonds, T. Kent, S. Lee, W. C. Trogler and A. C. Kummel, *J. Am. Chem. Soc.* , 2013, **135**, 14600-14609.
20. Y. Li and Q. Sun, *Scientific Reports*, 2014, **4**.
21. I. N. Remediakis, N. Lopez and J. K. Norskov, *Angew. Chem. Int. Ed.* , 2005, **44**, 1824-1826.
22. C. Harding, V. Habibpour, S. Kunz, A. N.-S. Farnbacher, U. Heiz, B. Yoon and U. Landman, *J. Am. Chem. Soc.*, 2009, **131**, 538-548.
23. D. Tang and C. Hu, *J. Phys. Chem. Lett.*, 2011, **2**, 2972-2977.
24. B. Delley, *The Journal of Chemical Physics*, 1990, **92**, 508-517.
25. B. Delley, *The Journal of Chemical Physics*, 2000, **113**, 7756-7764.
26. J. P. Perdew, K. Burke and M. Ernzerhof, *Physical Review Letters*, 1996, **77**, 3865-3868.
27. T. A. Halgren and W. N. Lipscomb, *Chemical Physics Letters*, 1977, **49**, 225-232.
28. G. Henkelman and H. Jónsson, *The Journal of Chemical Physics*, 2000, **113**, 9978-9985.
29. W. A. Brown, P. Gardner, M. P. Jigato and D. A. King, *J. Chem. Phys.*, 1995, **102**, 7277-7280.
30. C. I. Carlisle and D. A. King, *The Journal of Physical Chemistry B*, 2001, **105**, 3886-3893.
31. O. Byl, P. Kondratyuk and J. T. Yates, *J. Phys. Chem. B*, 2003, **107**, 4277-4279.
32. T. D. Chau, T. V. de Bocarmé and N. Kruse, *Catalysis Letters*, 2004, **98**, 85-87.
33. Y.-L. Zhao, M. D. Bartberger, K. Goto, K. Shimada, T. Kawashima and K. N. Houk, *J. Am. Chem. Soc.*, 2005, **127**, 7964-7965.
34. A. S. Mazheika, T. Bredow, O. A. Ivashkevich and V. E. Matulis, *J. Phys. Chem. C*, 2012, **116**, 25262-25273.
35. C. E. Dinerman and G. E. Ewing, *The Journal of Chemical Physics*, 1970, **53**, 626-631.
36. C. P. Vinod, J. W. Niemantsverdriet Hans and B. E. Nieuwenhuys, *Applied Catalysis A: General*, 2005, **291**, 93-97.
37. Z.-P. Liu, S. J. Jenkins and D. A. King, *Journal of the American Chemical Society*, 2004, **126**, 7336-7340.
38. N. Y. Dzade, A. Roldan and N. H. de Leeuw, *Physical Chemistry Chemical Physics*, 2014, **16**, 15444-15456.

RSC Advances Accepted Manuscript

39. X. F. Chen, J. M. Yan and Q. Jiang, *J. Phys. Chem. C*, 2014, **118**, 2122-2128.
40. J. w. Feng, Y. j. Liu and J. x. Zhao, *Journal of Molecular Graphics and Modelling*, 2015, **60**, 132-141.
41. X. Liu, Y. Sui, T. Duan, C. Meng and Y. Hanb, *Phys. Chem. Chem. Phys.*, 2014, **16**, 23584-23593.
42. Y. Tang, X. Dai, Z. Yang, L. Pan, W. Chen, D. Ma and Z. Lu, *Phys. Chem. Chem. Phys.*, 2014, **16**, 7887-7895.

RSC Advances Accepted Manuscript

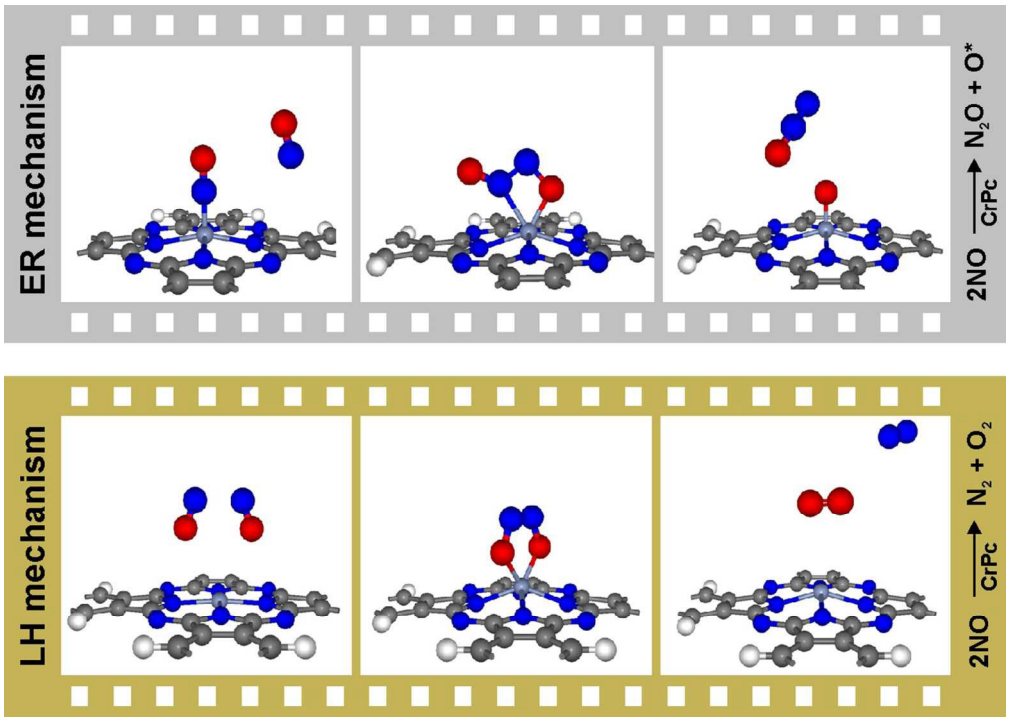

RSC Advances Accepted Manuscript